

Significant Anharmonicity of Thermal Transport in Amorphous Silica at High Temperature

Lei Yang and Bing-Yang Cao*

The anharmonicity of thermal transport in amorphous solids is underappreciated and inadequately understood, although considerable attention is paid to that of crystals. Herein, the anharmonic effects on the heat conduction of amorphous silica are investigated by combining the normal mode decomposition method with the Wigner transport equation. The existence of significant anharmonicity in amorphous silica, including temperature-dependent linewidths and frequency shifts of the vibrational modes, is demonstrated. By considering the anharmonic effects, the predicted temperature dependence of thermal conductivities at high temperatures agrees well with the increasing trend observed in experiments. The underlying mechanisms are further revealed. The anharmonic frequency shifts notably affect the strength of coupling between pairs of vibrational modes and dictate the positive temperature dependence, whereas the increasing linewidths with increasing temperature are of minor importance. This work contributes to the understanding of the anharmonicity of thermal vibrations and heat conduction in amorphous materials.

1. Introduction

Thermal transport in nonmetallic solids is contributed by atomic vibration through two conduction mechanisms, that is, particle-like propagating (population) and wave-like tunneling (coherence).^[1–5] Particle-like propagation is understood in the phonon picture and phonon Boltzmann transport equation (PBTE)^[6] combined with first-principle calculations has allowed quantitative prediction of its contribution to thermal conductivity (κ), in good agreement with experimental results for most crystalline materials.^[7–11] In the PBTE computational framework, significant anharmonic effects on κ from phonon scatterings and frequency shifts have been demonstrated in various crystalline semiconductors.^[12–18] On the other hand, coherences assume increasing significance when the linewidths of the vibrational modes are comparable with the interbranch spacings,^[4] that is, the case in complex crystals^[1,5,19,20] and


amorphous solids.^[21–29] Allen and Feldman^[30] first proposed a formulation for the coherences' contribution to κ by considering the off-diagonal elements of the velocity operator^[31,32] missed in PBTE. The Allen–Feldman (AF) theory considers the coupling of quasidegenerate vibrational modes and is appropriate for harmonic disordered solids. The role of anharmonicity has been regarded as a potential reason for the failure of the harmonic AF theory in some polymeric and chalcogenide glasses,^[25,33] but the anharmonicity of the vibrational modes is still little considered and inadequately explored in the computational study regarding the thermal transport in amorphous solids.

A widely investigated case for thermal transport is amorphous silica (a-SiO₂), with extensive applications in microelectronics.^[34–36] The temperature-

dependent κ of a-SiO₂ has been reported at a wide temperature range (1–1200 K) in various experimental studies,^[37–40] but the underlying mechanisms are complex and not fully understood. Zhu and Ertekin reproduced the plateau of the temperature-dependent κ at about 10 K by considering the coexisting populations' and coherences' conduction mechanisms in a model generalized from the Debye–Peierls and AF theory.^[41] At higher temperatures but below room temperature, κ is dominated by coherences and can be predicted by the quantum AF theory.^[42,43] However, above room temperature, the increasing κ with rising temperature is beyond the scope of the current theories. Although the Green–Kubo modal analysis (GKMA) method could lead to an agreeable prediction of κ with the experimental results at high temperatures,^[44] how the anharmonic frequency shifts and high-order interactions of the vibrational modes affect the heat conduction in a-SiO₂ is still unclear and deficiently understood.

In this article, we are devoted to investigating the anharmonic effects on thermal transport mechanisms in amorphous silica, especially at high temperatures. Using the molecular dynamics (MD)-based normal mode decomposition (NMD) method, we demonstrate the significant anharmonic frequency shifts and temperature-dependent linewidths of the vibrational modes in a-SiO₂. The unsolved positive temperature dependence of κ at high temperatures is reproduced by the Wigner transport equation (WTE). The underlying anharmonic effects and the coexisting particle-like and wave-like conduction mechanisms are further illustrated thoroughly.

L. Yang, B.-Y. Cao
Key Laboratory for Thermal Science and Power Engineering of Ministry of Education, Department of Engineering Mechanics
Tsinghua University
Beijing 100084, China
E-mail: caoby@tsinghua.edu.cn

 The ORCID identification number(s) for the author(s) of this article can be found under <https://doi.org/10.1002/pssr.202200217>.

DOI: 10.1002/pssr.202200217

2. Computational Method

Under single-mode relaxation time approximation of the WTE,^[4,42,45] κ is calculated by

$$\kappa = \frac{1}{VN_c} \sum_{\mathbf{q}} \sum_{s,s'} \frac{\omega_{\mathbf{q}s} + \omega_{\mathbf{q}s'}}{4} \left(\frac{C_{\mathbf{q}s}}{\omega_{\mathbf{q}s}} + \frac{C_{\mathbf{q}s'}}{\omega_{\mathbf{q}s'}} \right) \cdot \frac{v_{\mathbf{q},ss'}^2}{3} \cdot \frac{\frac{1}{2}(\Gamma_{\mathbf{q}s} + \Gamma_{\mathbf{q}s'})}{(\omega_{\mathbf{q}s} - \omega_{\mathbf{q}s'})^2 + \left(\frac{\Gamma_{\mathbf{q}s} + \Gamma_{\mathbf{q}s'}}{2}\right)^2} \quad (1)$$

in which V is the volume of the considered cell, $\omega_{\mathbf{q}s}$, $C_{\mathbf{q}s}$, and $\Gamma_{\mathbf{q}s}$ are angular frequency, specific heat, and linewidth, respectively, for each vibrational mode. In Equation (1), $v_{\mathbf{q},ss'}$ is the modulus of the velocity operator element averaged in three Cartesian directions for each pair of modes. Here, the average velocity operator is adopted since amorphous solids are always isotropic. The summation of the diagonal elements corresponds to the populations' contribution to κ , while the summation of the off-diagonal elements corresponds to the coherences', and both are operated over all the vibrational modes at $N_c \mathbf{q}$ points in reciprocal space. To calculate κ , the frequency and linewidth of each mode are needed. In general, the frequency and velocity operators are from harmonic lattice dynamics calculation and the linewidth is from the perturbation theory,^[10,46] including three- or higher-order scatterings. Here, the anharmonic properties of vibrational modes are predicted by the MD-based NMD method^[13,21,47] using DynaPhoPy, which has been tested by comparing the predicted linewidths and frequency shifts with experimental results of Raman spectroscopy.^[13] Full-order scatterings are included implicitly in the MD simulations performed using the LAMMPS package^[48] and the harmonic properties are calculated by phonopy.^[49] The atomic interactions in a-SiO₂ are described by Tersoff potential,^[50] which has been validated and widely used in MD studies^[44,51,52] for thermal transport of a-SiO₂. More computational details are presented in Section S1, Supporting Information.

3. Results and Discussion

The power spectra of a certain vibrational mode at 300 and 900 K are illustrated in **Figure 1a,b**, in which the mode linewidth ($\Gamma_{\mathbf{q}s}$), computed from the full width at half maximum of the spectra peak, and the frequency shift ($\Delta\omega_{\mathbf{q}s}^{\text{anh}}$), referring to the difference between anharmonic frequency ($\omega_{\mathbf{q}s}^{\text{anh}}$, the spectra peak position) and the harmonic frequency ($\omega_{\mathbf{q}s}^0$), are all marked. The negative frequency shift (softening) and power spectra broadening at higher temperatures are observed for the vibrational modes, shown in **Figure 1c,d**. The frequency shifts can be caused by thermal expansion or the anharmonic interactions, while the latter dominates at high temperatures.^[15] We also quantitatively evaluate the effects of thermal expansion using the quasiharmonic approximation. The frequency shifts due to thermal expansion are much slighter than those from anharmonicity due to the low thermal expansion coefficient of a-SiO₂. The calculation methods and results are presented in Section S3, Supporting Information. The softening effects due to the anharmonicity

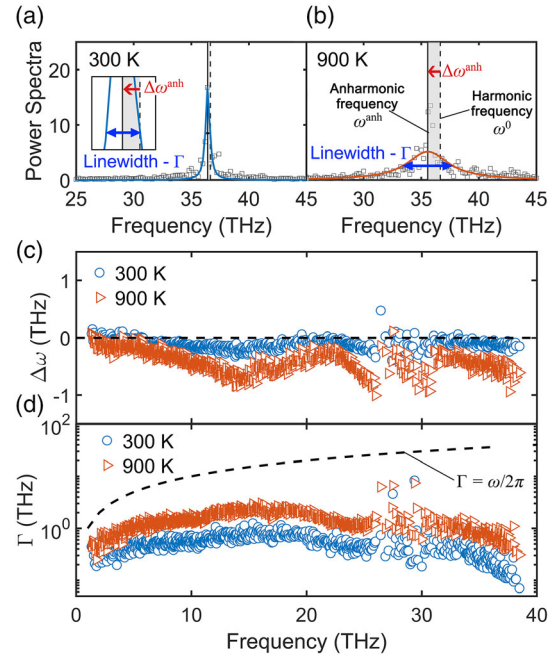


Figure 1. Power spectra of a vibrational mode of amorphous silica at a) 300 K and b) 900 K. c) The anharmonic frequency shifts ($\Delta\omega^{\text{anh}}$) and d) linewidths (Γ) of the vibrational modes in amorphous silica at various temperatures.

of vibrational modes observed in a-SiO₂ are similar to the situations in silicon^[13,15,18] and some thermoelectric semiconductors.^[53,54] The negative frequency shifts become more significant at higher temperatures, with the maximum shift reaching -1.0 THz and the average frequency shift equaling -0.40 THz at 900 K, much larger than -0.12 THz at 300 K. The linewidths also notably depend on temperature and become larger at higher temperatures due to stronger anharmonic interactions of the vibrational modes. We note that the Lorentzian spectral function approximation (LSFA) can still be used although the spectral energy deviates from the perfect Lorentzian to some extent because the criterion ($\Gamma < \omega/2\pi$) is satisfied,^[45,55] as shown in **Figure 1d**. Based on the results reported here, we conclude that the frequency shifts and linewidths of the vibrational modes in a-SiO₂ exhibit significant anharmonicity.

We also examine if the anharmonicity is important for the velocity operator by comparing the results based on the renormalized force constants at different temperatures. As seen in **Figure 2a,b**, the density distribution of all the velocity operator elements and the diagonal elements (equal to group velocity) versus mode frequency are both temperature-independent. Considering that the diagonal velocity operator elements are odd functions of \mathbf{q} , the \mathbf{q} -interpolation calculation is necessary and the convergence needs to be checked. The velocity operator elements calculated over the uniform $2 \times 2 \times 2$ and $3 \times 3 \times 3$ \mathbf{q} -mesh are illustrated in **Figure 2c,d**. Negligible differences exist and we attribute this to the large cell (with 300 atoms in this paper) used for the calculation. Thus, the $2 \times 2 \times 2$ \mathbf{q} -mesh is used to calculate κ of a-SiO₂ for lower computational cost. We also carried out supplementary studies to check the effects

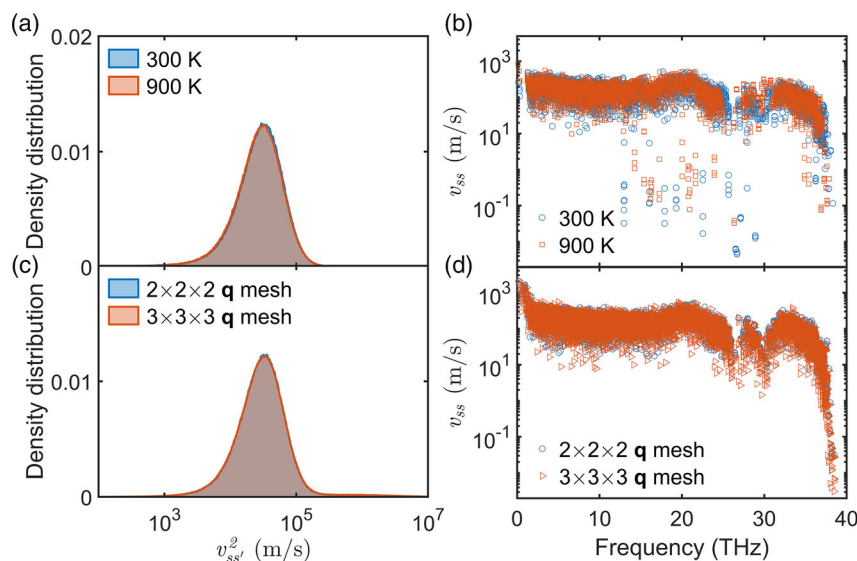


Figure 2. a) Density distribution of the square modulus of the velocity operator elements and b) the modulus of diagonal velocity operator elements at 300 and 900 K based on the renormalized force constants.^[13] c) Density distribution of the square modulus of the velocity operator elements and d) the modulus of diagonal velocity operator elements from the calculations over $2 \times 2 \times 2$ and $3 \times 3 \times 3$ q -mesh.

of the sample size, thermal expansion, and atom diffusion. The calculation details and results are given in S2–S4, Supporting Information. Three more a-SiO₂ samples (with 192, 648, and 1536 atoms) were generated and the predictions of κ using the WTE are size independent. The size independence is consistent with the measurement using frequency domain thermoreflectance.^[56] The effects of thermal expansion on thermal conductivities, calculated using the quasiharmonic method, are much slighter than anharmonic effects, due to the low coefficient of thermal expansion of a-SiO₂. At high temperatures, the atom diffusion might invalidate the approximation of the atomic equilibrium positions in WTE and even contribute to the thermal conductivity.^[57,58] By calculating the contribution to heat flux from atom diffusion, that is, kinetic part, in nonequilibrium molecular dynamics simulations from 300 to 1200 K, we confirm the neglectable effects of atom diffusion on thermal conductivity

(<0.5%). As for the possible change of the atomic equilibrium positions due to low activation energy^[59] and metastability,^[21] we add an annealing process when generating the amorphous structures of silica to remove such effects as much as possible. Here, the calculations are carried out up to 1200 K, lower than the glass transition temperature of a-SiO₂ (1480 K^[60]), to avoid possible significant effects of atom diffusion.

The anharmonic effects on κ are normally attributed to the change of the group velocity, specific heat, and lifetime under the PBTE framework for particle-like propagation for the vibrational modes.^[18] For a-SiO₂, the coherences' contribution is important and we extend the discussion by considering both conduction mechanisms. The temperature-dependent κ of a-SiO₂, including the contribution from populations and coherences, is calculated using the WTE formulation [Equation (1)]. The total κ is reported in **Figure 3a**, compared with

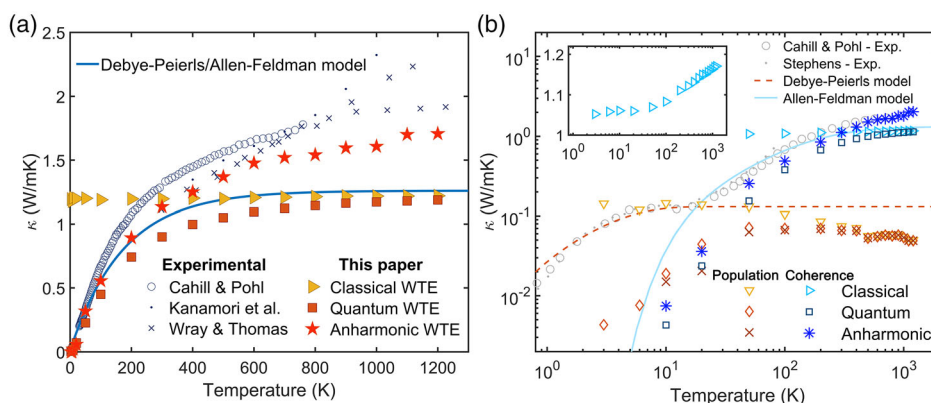


Figure 3. Temperature-dependent thermal conductivities of amorphous silica. a) Total thermal conductivity from the experiments,^[37,38,40] the generalized Debye–Peierls/Allen–Feldman model,^[41] and the calculation based on WTE in this article. b) Contribution to thermal conductivity from populations and coherences from the theoretical models^[41] and the calculation based on WTE in this article in logarithmic coordinates, compared with the experimental total thermal conductivity.^[39,40] The inset shows the coherences' conductivity from classical WTE in linear y-axis coordinates.

the results from the experiments^[37,38,40] and the generalized Debye–Peierls/Allen–Feldman (DPAF) model.^[41] Here, the classical, quantum, and anharmonic WTE are defined and used to predict the thermal conductivities to figure out the quantum and anharmonic effects. The definitions and the differences are listed in **Table 1**.

The results from classical WTE assume all the vibrational modes are fully excited, i.e., the mode-specific heat $C_{qs} = k_B$ (Boltzmann constant), while in quantum WTE

$$C_{qs} = k_B \left[\frac{\hbar\omega/2k_B T}{\sinh(\hbar\omega/2k_B T)} \right]^2 \quad (2)$$

which is from considering the quantum Bose–Einstein distribution for the vibrational modes. The difference between quantum and classical WTE diminishes with the temperature rising and the difference of $\kappa < 0.1 \text{ W mK}^{-1}$ above 700 K. These results at high temperatures are also in good agreement with the direct MD simulations,^[51,61,62] in which the quantum effect is ignored. By considering the quantum effects, our calculation and the DPAF model both capture the temperature dependence below room temperature, but fail to describe the increasing trend at higher temperatures observed in the experiments. This increasing trend is also beyond the description of WTE with three-order anharmonic scatterings considered.^[42] Our results from quantum and classical WTE rely on the linewidths predicted by the MD-based NMD method and include the full-order scatterings. The failure of the WTE including three-order or full-order anharmonic scatterings indicates that the discrepancy between theoretical and experimental κ at high temperatures is not caused by the omission of the higher-order anharmonic interactions for calculation of linewidths. We further consider the effects of anharmonic frequency shifts in WTE and the results (marked as anharmonic WTE) accord closely with the temperature dependence of κ observed in the experiments. The differences between the results from anharmonic and quantum WTE are also notable, about 0.24 W mK^{-1} (26%) at 300 K and 0.52 W mK^{-1} (44%) at 1200 K. These findings indicate that the anharmonic frequency shift is a dominant factor for the increasing trend of κ at high temperatures. The GKMA method, based on MD simulations, also well reproduced the increasing trend and used the same potential.^[44] The results from anharmonic WTE are smaller than those of GKMA by $0.15\text{--}0.3 \text{ W mK}^{-1}$ from 300 to 1200 K. The

difference might be due to the deviation from the perfect Lorentzian of the mode energy spectral^[63,64] and the higher-order heat flux^[65] that are implicitly included in the MD simulation but not included in WTE. Also, the quantum-specific heat correction in GKMA, excluding the difference between each pair of modes in coherences' contribution, may cause a discrepancy. These effects might be further explored quantitatively in the future, and we focus on the significant effects and the underlying mechanisms of the anharmonic frequency shifts in this article.

Populations' and coherences' contributions to κ are also quantified at a wider temperature range and shown under logarithmic coordinates in Figure 3b. The predicted populations and coherences' κ from quantum WTE agree with those from the Debye–Peierls and Allen–Feldman models, respectively, regarding both the magnitude and the temperature dependence. The coherences' contribution decreases faster with the decreasing temperature, and the competence of the coexisting conduction mechanisms leads to the plateau at about 10 K. Above 100 K, the coherences' contribution is orders larger than that from populations, similar to the most cases for amorphous solids in which coherences dominate the heat conduction. Compared with the results considering the anharmonic frequency shifts, we additionally demonstrate that the increasing κ with rising temperature is due to coherences' anharmonicity and the frequency shifts almost have no influence on populations' contribution. The classical WTE excludes the quantum effects and well reflects the effects from temperature-dependent mode linewidths on κ . The classical results show that the increasing linewidths of the vibrational modes at higher temperatures result in the smaller populations' κ but slightly larger coherences' contribution (see the inset of Figure 3b). Nevertheless, the dominant coherences' contribution and much more significant effects from quantum distribution and anharmonic frequency shifts overshadow the effects on κ from the temperature-dependent mode linewidths in a-SiO₂.

To further investigate the underlying mechanisms of the anharmonicity of thermal transport of a-SiO₂, we calculate the mode resolved thermal conductivity (κ_{qs}) by the decomposing coherences' contribution from each pair of vibrational modes weighted by specific heat, and then the total κ can be calculated by a compact form

$$\kappa = \frac{1}{N_c} \sum_{qs} \kappa_{qs} = \frac{1}{VN_c} \sum_{qs} C_{qs} D_{qs} \quad (3)$$

By introducing the mode diffusivity (D_{qs}) in Equation (3), the effects from specific heat and the coupling strength of each pair of vibrational modes can be decoupled. Here, the diffusivity represents the coupling strength of coherences' coupling, similar to the diffusivity predicted by the AF theory, but including the anharmonicity and without empirical parameters. Temperature-dependent linewidths and frequency shifts are two important factors for the coherences' coupling strength. **Figure 4a–c** show the mode diffusivities of a-SiO₂ with or without considering the anharmonic frequency shifts at various temperatures. The stronger coupling strength at higher temperatures is observed, which is due to the increasing mode linewidths. At 300 and 900 K, anharmonic frequency shifts cause stronger coherences' coupling, especially for the high-frequency modes,

Table 1. Definitions of classical WTE, quantum WTE, and anharmonic WTE.

	Definition
Classical WTE	Considering neither quantum effect nor anharmonic frequency shifts $C_{qs} = k_B$, $\omega_{qs} = \omega_{qs}^0$
Quantum WTE	Considering quantum effect but without considering anharmonic frequency shifts $C_{qs} = k_B \left[\frac{\hbar\omega_{qs}/2k_B T}{\sinh(\hbar\omega_{qs}/2k_B T)} \right]^2$, $\omega_{qs} = \omega_{qs}^0$
Anharmonic WTE	Considering both quantum effect and anharmonic frequency shifts $C_{qs} = k_B \left[\frac{\hbar\omega_{qs}/2k_B T}{\sinh(\hbar\omega_{qs}/2k_B T)} \right]^2$, $\omega_{qs} = \omega_{qs}^{anh} = \omega_{qs}^0 + \Delta\omega_{qs}^{anh}$

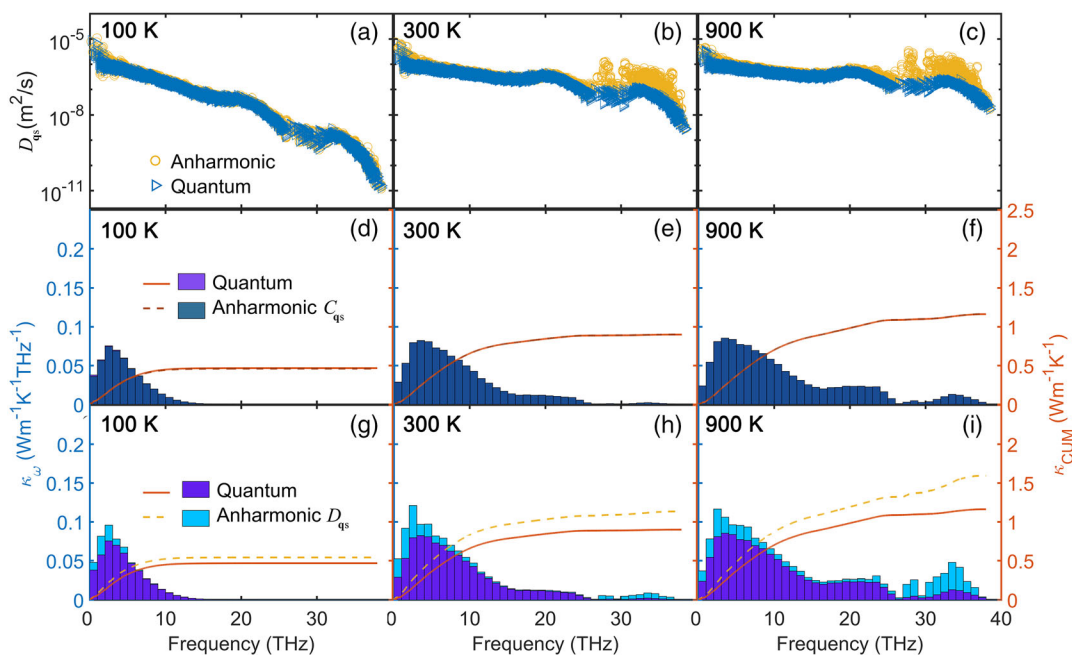


Figure 4. Diffusivities (D_i) calculated with and without including anharmonic frequency shifts at a) 100 K, b) 300 K, and c) 900 K. Thermal conductivity density of states (κ_ω) and cumulative total thermal conductivity (κ_{cum}) from WTE, at d) 100 K, e) 300 K, and f) 900 K, with and without considering anharmonic frequency shift in the specific heat (C_{qs}) of each vibrational mode. κ_ω and κ_{cum} from WTE, at g) 100 K, h) 300 K, and i) 900 K, with and without considering anharmonic frequency shift in the diffusivity (D_{qs}) of each vibrational mode.

corresponding to the non-negligible contribution of locons observed in previous direct MD simulation.^[44] Our calculation further demonstrates that the contribution highly depends on the anharmonic frequency shifts. As for the specific heat, the temperature dependence is related to the frequency shifts and can be interpreted from Equation (2), based on considering the quantum Bose–Einstein distribution for the vibrational modes. The separate anharmonic effects through specific heat and coherences coupling strength can be quantified by only considering the frequency shifts in a mode-specific heat and diffusivity, as shown by the thermal conductivity density of states (κ_ω) and cumulative thermal conductivity (κ_{cum}) at various temperatures in Figure 4d–i. Considering anharmonic frequency shifts result in almost the same κ_ω and κ_{cum} with those from the regular WTE. This suggests that the anharmonicity of mode-specific heat is of little importance and is consistent with the good agreement between the specific heat calculated without considering the frequency shifts and experimental results.^[42] In contrast, the anharmonicity of coherences’ coupling has a substantial effect on κ . The effect originates from all the vibrational modes and becomes more dramatic at higher temperatures, especially for the high-frequency modes. The findings here demonstrate the necessity of considering anharmonic effects for predicting coherences’ conductivity.

4. Conclusion

To conclude, we combined the NMD techniques and the unified WTE formulation, which can account for the coexisting

populations and coherences’ conduction mechanisms, as well as the anharmonicity, to investigate the thermal transport in amorphous silica. Significant anharmonicity, including the temperature-dependent vibrational mode linewidths and anharmonic frequency shifts, exists in a-SiO₂. The linewidths become larger and the negative frequency shifts become more dramatic with increasing temperature. The larger frequency shifts lead to higher coherences’ coupling strength and dictate the increasing temperature dependence of κ at high temperatures, while the varied mode linewidths have neglectable effects on both populations’ and coherences’ conductivity. Our findings offer new insights into heat conduction in amorphous solids regarding the anharmonicity and are also instructive for low- κ crystals and other disordered materials, in which coherences are important for thermal transport.

Supporting Information

Supporting Information is available from the Wiley Online Library or from the author.

Acknowledgements

This work was supported by the National Natural Science Foundation of China (nos. 51825601 and U20A20301).

Conflict of Interest

The authors declare no conflict of interest.

Data Availability Statement

The data that support the findings of this study are available from the corresponding author on reasonable request.

Keywords

amorphous silica, anharmonicity, coherence, thermal transport

Received: June 17, 2022

Revised: August 7, 2022

Published online: September 4, 2022

- [1] Y. Luo, X. Yang, T. Feng, J. Wang, X. Ruan, *Nat. Commun.* **2020**, *11*, 2554.
- [2] S. Mukhopadhyay, D. S. Parker, B. C. Sales, A. A. Puretzy, M. A. McGuire, L. Lindsay, *Science* **2018**, *360*, 1455.
- [3] L. Isaeva, G. Barbalinardo, D. Donadio, S. Baroni, *Nat. Commun.* **2019**, *10*, 3853.
- [4] M. Simoncelli, N. Marzari, F. Mauri, *Nat. Phys.* **2019**, *15*, 809.
- [5] Z. Zhang, Y. Guo, M. Bescond, J. Chen, M. Nomura, S. Volz, *Phys. Rev. Lett.* **2022**, *128*, 015901.
- [6] R. Peierls, *Ann. Phys.* **1929**, *395*, 1055.
- [7] G. Fugallo, M. Lazzeri, L. Paulatto, F. Mauri, *Phys. Rev. B* **2013**, *88*, 045430.
- [8] W. Li, J. Carrete, N. A. Katcho, N. Mingo, *Comput. Phys. Commun.* **2014**, *185*, 1747.
- [9] J. Carrete, B. Vermeersch, A. Katre, A. van Roekeghem, T. Wang, G. K. H. Madsen, N. Mingo, *Comput. Phys. Commun.* **2017**, *220*, 351.
- [10] H. Bao, J. Chen, X. Gu, B. Cao, *ES Energy Environ.* **2018**, *1*, 16.
- [11] A. J. H. McGaughey, A. Jain, H.-Y. Kim, *J. Appl. Phys.* **2019**, *125*, 011101.
- [12] O. Hellman, I. A. Abrikosov, S. I. Simak, *Phys. Rev. B* **2011**, *84*, 180301.
- [13] A. Carreras, A. Togo, I. Tanaka, *Comput. Phys. Commun.* **2017**, *221*, 221.
- [14] Y. Xia, K. Pal, J. He, V. Ozoliņš, C. Wolverton, *Phys. Rev. Lett.* **2020**, *124*, 065901.
- [15] D. S. Kim, H. L. Smith, J. L. Niedziela, C. W. Li, D. L. Abernathy, B. Fultz, *Phys. Rev. B* **2015**, *91*, 014307.
- [16] S. Tanusilp, M. Kumagai, Y. Ohishi, N. Sadayori, K. Kurosaki, *Physica Status Solidi RRL* **2022**, *16*, 2100482.
- [17] T. Feng, L. Lindsay, X. Ruan, *Phys. Rev. B* **2017**, *96*, 161201.
- [18] T. Feng, X. Yang, X. Ruan, *J. Appl. Phys.* **2018**, *124*, 145101.
- [19] W. D. C. B. Gunatilleke, R. Juneja, O. P. Ojo, A. F. May, H. Wang, L. Lindsay, G. S. Nolas, *Phys. Rev. Mater.* **2021**, *5*, 085002.
- [20] X. Yang, J. Tiwari, T. Feng, *Mater. Today Phys.* **2022**, *24*, 100689.
- [21] J. M. Larkin, A. J. H. McGaughey, *Phys. Rev. B* **2014**, *89*, 144303.
- [22] F. DeAngelis, M. G. Muraleedharan, J. Moon, H. R. Seyf, A. J. Minnich, A. J. H. McGaughey, A. Henry, *Nanoscale Microscale Thermophys. Eng.* **2019**, *23*, 81.
- [23] G. C. Sosso, V. L. Deringer, S. R. Elliott, G. Csányi, *Mol. Simul.* **2018**, *44*, 866.
- [24] G. C. Sosso, D. Donadio, S. Caravati, J. Behler, M. Bernasconi, *Phys. Rev. B* **2012**, *86*, 104301.
- [25] L. Yang, B.-Y. Cao, *J. Phys. D: Appl. Phys.* **2021**, *54*, 505302.
- [26] K. Aryana, D. A. Stewart, J. T. Gaskins, J. Nag, J. C. Read, D. H. Olson, M. K. Grobis, P. E. Hopkins, *Nat. Commun.* **2021**, *12*, 2817.
- [27] N. Tambo, Y. Liao, C. Zhou, E. M. Ashley, K. Takahashi, P. F. Nealey, Y. Naito, J. Shiomi, *Sci. Adv.* **2020**, *6*, eabc0075.
- [28] J. L. Feldman, M. D. Kluge, P. B. Allen, F. Wooten, *Phys. Rev. B* **1993**, *48*, 12589.
- [29] P. B. Allen, J. L. Feldman, J. Fabian, F. Wooten, *Philos. Mag. B* **1999**, *79*, 1715.
- [30] P. B. Allen, J. L. Feldman, *Phys. Rev. B* **1993**, *48*, 12581.
- [31] R. J. Hardy, *Phys. Rev.* **1963**, *132*, 168.
- [32] P. B. Allen, J. L. Feldman, *Phys. Rev. Lett.* **1989**, *62*, 645.
- [33] S. Shenogin, A. Bodapati, P. Keblinski, A. J. H. McGaughey, *J. Appl. Phys.* **2009**, *105*, 034906.
- [34] M. C. Wingert, J. Zheng, S. Kwon, R. Chen, *Semicond. Sci. Technol.* **2016**, *31*, 113003.
- [35] P. Li, Y. Song, X. Zuo, *Phys. Status Solidi RRL* **2019**, *13*, 1800547.
- [36] W. Zhou, Y. Cheng, K. Chen, G. Xie, T. Wang, G. Zhang, *Adv. Funct. Mater.* **2020**, *30*, 1903829.
- [37] K. L. Wray, T. J. Connolly, *J. Appl. Phys.* **1959**, *30*, 1702.
- [38] H. Kanamori, N. Fujii, H. Mizutani, *J. Geophys. Res.* **1968**, *73*, 595.
- [39] R. B. Stephens, *Phys. Rev. B* **1973**, *8*, 2896.
- [40] D. G. Cahill, R. O. Pohl, *Solid State Commun.* **1989**, *70*, 927.
- [41] T. Zhu, E. Ertekin, *Phys. Rev. B* **2016**, *93*, 155414.
- [42] M. Simoncelli, in *Thermal Transport Beyond Fourier, And Beyond Boltzmann*, École Polytechnique Fédérale de Lausanne, Lausanne, France **2021**.
- [43] Y. Zhou, *J. Appl. Phys.* **2021**, *129*, 235104.
- [44] W. Lv, A. Henry, *Sci. Rep.* **2016**, *6*, 35720.
- [45] M. Simoncelli, N. Marzari, F. Mauri, arxiv:2112.06897 [Cond-Mat], **2021**.
- [46] G. Barbalinardo, Z. Chen, N. W. Lundgren, D. Donadio, *J. Appl. Phys.* **2020**, *128*, 135104.
- [47] T. Sun, D.-B. Zhang, R. M. Wentzcovitch, *Phys. Rev. B* **2014**, *89*, 094109.
- [48] S. Plimpton, *J. Comput. Phys.* **1995**, *117*, 1.
- [49] A. Togo, I. Tanaka, *Scr. Mater.* **2015**, *108*, 1.
- [50] S. Munetoh, T. Motooka, K. Moriguchi, A. Shintani, *Comput. Mater. Sci.* **2007**, *39*, 334.
- [51] W. Zhu, G. Zheng, S. Cao, H. He, *Sci. Rep.* **2018**, *8*, 10537.
- [52] H. Gu, H. Wang, *Comput. Mater. Sci.* **2018**, *144*, 133.
- [53] Y. Wang, B. Qiu, A. J. H. McGaughey, X. Ruan, X. Xu, *J. Heat Transfer* **2013**, *135*, 091102.
- [54] Y. Xiao, C. Chang, Y. Pei, D. Wu, K. Peng, X. Zhou, S. Gong, J. He, Y. Zhang, Z. Zeng, L.-D. Zhao, *Phys. Rev. B* **2016**, *94*, 125203.
- [55] G. Caldarelli, M. Simoncelli, N. Marzari, F. Mauri, L. Benfatto, arxiv:2202.02246 [Cond-Mat], **2022**.
- [56] K. T. Regner, D. P. Sellan, Z. Su, C. H. Amon, A. J. H. McGaughey, J. A. Malen, *Nat. Commun.* **2013**, *4*, 1640.
- [57] E. L. Williams, *J. Am. Ceram. Soc.* **1965**, *48*, 190.
- [58] J. Moon, *J. Appl. Phys.* **2021**, *130*, 055101.
- [59] Y. Fan, T. Iwashita, T. Egami, *Nat. Commun.* **2017**, *8*, 15417.
- [60] B. Deng, Y. Shi, F. Yuan, *Materialia* **2020**, *12*, 100752.
- [61] L. Ercole, in *Ab Initio Simulation Of Heat Transport In Silica Glass*, Scuola Internazionale Superiore di Studi Avanzati, Trieste TS, Italy **2018**.
- [62] E. Martin, G. Ori, T.-Q. Duong, M. Boero, C. Massobrio, *J. Non-Cryst. Solids* **2022**, *581*, 121434.
- [63] Z. Zhang, Y. Guo, M. Bescond, J. Chen, M. Nomura, S. Volz, *NPJ Comput. Mater.* **2022**, *8*, 96.
- [64] Đ. Dangić, O. Hellman, S. Fahy, I. Savić, *NPJ Comput. Mater.* **2021**, *7*, 57.
- [65] T. Sun, P. B. Allen, *Phys. Rev. B* **2010**, *82*, 224305.